UPPSALA
UNIVERSITET

Developing a protocol for RT-qPCR of wing-tissue gene expression and investigating the dynamics of photoperiodically induced polyphenism in the water strider *Gerris buenoi*

Elin Andersson

Degree project in biology, Master of science (2 years), 2023
Examensarbete i biologi 30 hp till masterexamen, 2023
Biology Education Centre and Department of Ecology and Genetics, Uppsala University
Supervisor: Arild Husby
External opponent: David Manyara

Table of contents

Abstract

Wing polyphenism in insects is a type of phenotypic plasticity where environmental factors trigger the development of a set of discrete wing morphologies. In the water strider *Gerris buenoi*, photoperiods are the main environmental cue that trigger wing morph determination. The genetic mechanisms connecting environmental cues and the determination of wing morph in *G. buenoi* are not clear. However, recent experimental work suggests that engagement of the Hippo pathway via ecdysone signalling is a promising model for further investigation. In this study, a reverse-transcription quantitative PCR (RT-qPCR) protocol was developed, aimed at elucidating this potential transduction pathway by quantifying gene expression of Fat, Dachsous, Yorkie, EcR, E75 and E74. This was done using melt curve analysis, gel electrophoresis, sequencing of RT-qPCR products and qPCR standard curves. Additionally, wing morph distribution in extreme and intermediate photoperiods were examined. Wing morph proportions were significantly different between adults emerging in the intermediate photoperiods 15.30:8.30 and 15:9 (hours light : hours dark). An effect of sex was observed, with a higher probability of males becoming long-winged compared to females. This has likely evolved as a result of a dispersal-reproduction trade-off. Taken together, this study provided insight for future investigations of periodically induced wing morph determination and its genetic mechanisms in *G. buenoi* that will contribute to the understanding of phenotypic plasticity.

Introduction

Phenotypic plasticity and wing polyphenism

The ability to adapt to the environment is key to the survival of organisms and phenotypic plasticity is an important property of species that enables within-generation adaptation. Phenotypic plasticity can be defined as the ability of a single genome to generate different forms of behaviour, morphology and physiology depending on the environment (West-Eberhard 2003, Simpson *et al.* 2011). This plasticity can be continuous, with gradual phenotypic change, or it can be discontinuous, with discrete phenotypic variants (Nijhout 2003).

A well-studied example of discontinuous phenotypic plasticity is wing polyphenism in insects (Nijhout 2003, West-Eberhard 2003). Here, irreversible alternative wing length morphologies arise in the same population and life stage in response to certain environmental cues (West-Eberhard 2003). Wing polyphenism is relatively common in insects and is likely an adaptation to life in heterogeneous environments (Zhang *et al.* 2019). In particular, there is a trade-off between dispersal and reproduction (Roff 1986, Zera & Denno 1997) where producing and maintaining flight capability costs a lot of energy which in favourable conditions, where flight is not necessary, could be used in favour of production of offspring instead. Generally, short-winged females have higher fecundity than long-winged females (Roff 1986, Zera & Denno 1997), for example through earlier start of egg production, as found in crickets (Roff 1984). Studies of wing polyphenism contribute to the understanding of how the environment produces phenotypic variation and how phenotypic plasticity has evolved.

The environmental cues that trigger determination of wing length in wing-polyphenic insects as well as the genetic mechanism behind it varies between different species (Xu *et al.* 2015, Fawcett *et al.* 2018, Gudmunds *et al.* 2022). For example, studies of the brown planthopper (*Nilaparvata lugens*), the pea aphid (*Acyrthosiphon pisum*) and crickets (Gryllidae) have demonstrated that host plant quality, rearing density, temperature and photoperiod can act individually, or interact, to affect wing morph determination (Zhang *et al.* 2019). Water striders (Hemiptera) are semi-aquatic bugs that show substantial variation in occurrence of wing polyphenism between lineages (Andersen 1993). Some species are phenotypically plastic and able to develop long (macropterous) and short (micropterous) wing morphs, other species are monomorphic wingless or long-winged (Andersen 1993). In several water strider species, photoperiod has been shown to be a strong environmental cue that regulates wing morph determination (Vepsäläinen 1971, Spence 1989, Harada & Numata 1993, Gudmunds *et al.* 2022) but nymphal rearing density and temperature can also play a significant role (Vepsäläinen 1974, Harada & Numata 1993, Fairbairn & King 2009, Han 2020, Gudmunds *et al.* 2022). For example, in the species *Gerris buenoi*, short-day (e.g. 12 h light : 12 h dark) conditions leads to induction of the long-winged phenotype and the short-winged phenotype is induced in long-day conditions (e.g. 18 h light : 6 h dark). However, long-winged individuals can also be induced by high density in 18:6. In addition to the long-winged and short-winged morphs, an intermediate wing phenotype (mesopterous) can be observed in *G. buenoi*, albeit in comparably low frequencies (Gudmunds *et al.* 2022).

The molecular and physiological regulation of wing polyphenism

How environmental cues are transduced to the molecular pathways causing wing morph induction in water striders remains unclear (Gudmunds 2023). However, it is likely that the induction pathway includes hormones which have the ability to transfer signals from

environmental-sensing organs in the brain to the location of action via the circulatory system, thereby activating molecular pathways involved in wing morph development (Nijhout 2003, Zera 2003, Gotoh *et al.* 2015, Zhang *et al.* 2019). These molecular pathways seem to vary between insects. For example, in some hemipterans, the nutrient sensing insulin/insulin-like receptor signalling (IIS) pathway has been shown to be involved in wing morph determination (Xu *et al.* 2015, Lin *et al.* 2018). Recently, Gudmunds *et al*. (2022) sought out to investigate a potential role of the IIS in wing form determination in the water strider *G. buenoi* and their results suggested that the genes in this pathway (*InR1*, *InR2*, *InR1-like*, *FOXO*) are not involved (Gudmunds *et al.* 2022). Another candidate was the Fat/Hippo pathway; this conserved pathway had been proposed to link changes in the environment to plastic growth of organs, via morphogens and hormones (Gotoh *et al.* 2015). Transcriptomic data from *G. buenoi* wing-tissue showed that Hippo signalling genes *Fat* (*Ft*), *Dachsous* (*Ds*) and *Yorkie* (*Yki*) was downregulated during late instar (nymphal developmental stage) 5 in striders reared in long photoperiods and RNAi knock-down supported the involvement of the Hippo pathway in wing morph determination (Gudmunds 2023).

The main endocrine pathways that have been shown to regulate wing polyphenism in insects are the juvenile hormone (JH) and the steroid hormone ecdysone pathways (Iwanaga & Tojo 1986, Vellichirammal *et al.* 2016, Vellichirammal *et al.* 2017, Zhang *et al.* 2019). Of these hormones, ecdysone is the main candidate to regulate wing morph determination in *G. buenoi*, as small but significant shifts in wing morph frequencies were found after knock-down of the ecdysone receptor EcR using RNAi. Additionally, RNA sequencing data showed differences in the expression of ecdysone-regulated genes such as EcR, E74 and E75 in wing-progenitor tissue between nymphs reared in 12:12 and 18:6 photoperiods, suggesting a role in wing morph determination (Gudmunds 2023). Despite these results, additional studies are required to conclusively demonstrate that ecdysone is the hormone that mediates the environmental signal to the growing wing tissue in *G. buenoi*.

Reverse-transcription quantitative PCR as a tool for studying differential gene expression

Fluorescence-based quantitative PCR (qPCR) (Higuchi *et al.* 1992, Higuchi *et al.* 1993, Wittwer *et al.* 1997) is used to indirectly measure the absolute or relative amount of a target DNA sequence within a sample (Bustin *et al.* 2009). In this study, the relative quantity of mRNA in RNA extracts from water striders was investigated. This is achieved through the coupling of reverse-transcription, where complementary DNA (cDNA) is synthesised from extracted mRNA, with qPCR reactions. In qPCR, fluorescent dyes are used to monitor the amplification of the cDNA. During the exponential phase, the cDNA amplification is directly proportional to the initial cDNA concentration and the detection should take place during this time (Biassoni & Raso 2014).

The quantification cycle (C_q) (also called threshold cycle) is the cycle in which the fluorescence of a reaction reaches above a certain (chosen) threshold. This threshold is set above the background noise, at the exponential phase, and is the same for all reactions during one run (Bustin & Nolan 2004, Biassoni & Raso 2014). These C_q values are then used to determine the amount of target sequence in the sample; a higher C_q value could indicate a higher amount of this target in the sample. However, the primer efficiency also needs to be accounted for. The range of C_q values that is considered reliable varies between reactions and can be determined for each reaction using dilution series from which one can create standard curves (or calibration curves). Standard curves are the C_q values plotted against initial cDNA concentration on logarithmic scale. Analysis of how the data fit the linear regression model

will give an indication of the range of reliable C_q values (Bustin *et al.* 2009) and consequently, the range of adequate input cDNA concentrations.

In an RT-qPCR experiment, one needs to take primer efficiency (also called amplification efficiency or PCR efficiency) into consideration. Primer efficiency represents how many copies are replicated during each PCR cycle; an ideal efficiency of 100% means that the amount of template doubles with each cycle (Biassoni & Raso 2014, Svec *et al.* 2015). In the end, the quantity of the target genes relative to the reference genes can be determined. Therefore, reference genes that are stable across treatments are needed to determine the effect of treatments on the genes of interest (Bustin *et al.* 2009).

The qPCR products need to be validated to make sure that the target sequence and nothing else was amplified, especially when using non-specific dyes like SYBR Green. One way to identify qPCR products is melt curve analysis: the amplification products are heated until dissociation of dsDNA occurs, at which point the fluorescence decreases. By taking the first derivative of melt curves, one can transform them into melt peaks (Ririe *et al.* 1997, Bustin & Nolan 2004). Another way of validating qPCR products are gel electrophoresis and DNA sequencing of qPCR products (Bustin *et al.* 2009).

Although RT-qPCR is a powerful functional genetic tool to investigate gene expression, there are many sources of variation using this method, not just between laboratories and protocols but also between individual runs and individual reactions. Therefore, calibration between plates, standardisation using carefully picked reference genes and correct interpretation of data analysis are of utmost importance to make valid conclusions (Bustin & Nolan 2004, Bustin *et al.* 2009). To not waste precious, low concentration RNA samples, validation of the method before starting experiments is essential.

Aim

The aim of this study was to develop an experimental protocol for investigating gene expression differences underlying wing morph determination in the water strider *G. buenoi*. Such investigations will increase our understanding of the molecular mechanism behind wing polyphenism in insects and how environmental changes confer developmental plasticity. We did this by exploring wing morph distribution in extreme and intermediate photoperiods and by developing methods for RT-qPCR.

Firstly, we examined the wing morph distribution of *G. buenoi* individuals reared in the photoperiods 12:12 (hours light : hours dark) and 18:6, known from previous studies to induce predominantly macropterous and micropterous individuals, respectively (Gudmunds *et al.* 2022). Secondly, we investigated the dynamics of wing morph determination in intermediate photoperiods 15.30:8.30 and 15:9, to find the critical photoperiod that gives rise to a close to 50:50 distribution of long-winged and short-winged individuals. These experiments aimed to add to the understanding of photoperiodically induced wing polyphenism and to explore the difference in wing morph proportions between sexes. Thirdly, we aimed to develop a protocol for RT-qPCR of wing-tissue gene expression where the functionality of primers were examined, the range of appropriate sample concentrations were determined and stability of reference genes were explored.

Materials and methods

Water strider rearing

The *Gerris buenoi* individuals used for this project originated from a population collected from a pond in Toronto, Ontario, Canada. Since then, they have been cultivated and outcrossed in the lab. Stock population striders were kept in large plastic boxes (38 × 51 cm) at room temperature in an 18:6 photoperiod. They were fed at least three times a week with frozen crickets *ad libitum* and were provided Styrofoam strips to rest and lay eggs on. Nymphs were hatched in separate, medium sized boxes. Striders used for experiments were moved from stock population to their respective photoperiod during instar 1, at the latest. They were kept in light rooms set to 25 °C and a specific photoperiod. The boxes were cleaned regularly, and the water surface was kept clean.

Striders used for the qPCR assay as well as wing morph frequency determination in 12:12 and 18:6 were kept in medium and small sized plastic boxes (38 × 19 cm and 19 × 26 cm, respectively) and kept at a density of ~25-35 striders/medium box until instar 5, from which the density was strictly kept at a maximum of 48.1 cm^2/strider to avoid density affecting wing morph determination. They were fed *ad libitum* with frozen crickets at least five days a week. Once they became instar 5, they were fed every day to equalise developmental time in sampled individuals. During instar 5 sampling, feeding was done in the morning before sampling in the afternoon.

Striders used for the wing frequency experiments in intermediate photoperiods 15:9 and 15.30:8.30 (15 h 30 min light : 8 h 30 min dark) were kept in medium and small sized boxes and fed 5 times a week until reaching adulthood. The rearing density was kept at a maximum of 20.6 cm^2/strider from the time of reaching instar 4.

The effect of photoperiod on wing morph determination

Striders reared in 12:12 (n=56) and 18:6 (n=65) were kept at the same conditions as the individuals used for qPCR assay sampling. When they reached adulthood, their wing morphs were determined by eye. If this was too difficult, they were scored later on using a microscope. All scored individuals were kept in 70% ethanol. Macropterous morph was defined as forewing length being equal to or longer than the sixth abdominal segment, micropterous was defined as forewing length being equal to or shorter than the first segment, and mesopterous was defined as forewing length being in between these (Gudmunds *et al.* 2022).

Striders reared in intermediate photoperiods 15:9 and 15.30:8.30 were kept at an approximately constant density from the time of reaching instar 4 and a constant feeding regime (see Strider rearing). They were scored once reaching adulthood. All individuals in one box were scored at the same time, when all individuals had become adults (with the exception of 1-2 striders), to keep rearing density as constant as possible. Determination of wing morph and sex was done as described above. The wing morph and sex of a total of 295 striders and 324 striders were scored in 15:9 and 15.30:8.30, respectively.

One 15:30:8.30 box (n=9) with obvious deviant wing morph proportions between macropterous, micropterous and mesopterous morphs were counted as an outlier and not included in χ^2 tests. Generalised linear mixed effects models (GLMER) were fitted to the data, with wing morph as a binary response variable and sex and photoperiod as predictors. Batch effects of different boxes were accounted for by adding boxes as a random effect. Since

the frequencies of mesopterous individuals were too small for these statistical tests, micropterous and mesopterous individuals were grouped together.

Sampling for qPCR assay

Striders were sampled from two extreme photoperiods (12:12, promoting macropterous individuals, and 18:6, promoting micropterous individuals). Sampling was done at the developmental time point Day 2 of instar 5. Day 1 was defined as the day of morphing into instar 5. Each sampling session was done within the same three-hour time span in the afternoon (~14.00-17-00), after which Instar 5:s that were destined to be sampled later were isolated from the original growth box. Five and eight females in Day 2 of instar 5 were sampled from photoperiod 18:6 (sample F18.2.1) and 12:12 (sample F12.2.2), respectively. This provided one biological replicate for each photoperiod at this time point to be used for downstream qPCR.

The sampling process was carried out as follows: the sex of an individual was determined by eye and then moved into an empty tube that was immediately submerged into liquid nitrogen for 3 seconds. Tubes were kept in the liquid nitrogen tank until the sampling session was over and then stored at -70 °C. Samples were kept at -70 °C until the start of wing bud dissection.

RNA extraction and purification

The left and right fore-wing buds were dissected under a microscope in ice cold 1X PBS with 1% Tween. Dissected wing buds were put in 10 µl Trizol and were thoroughly homogenised using the dissection tweezers. 480 µl of Trizol was added and tubes were vortexed. The samples were incubated on ice for ~1 hour and then stored in -20 °C until RNA extraction.

After defrosting and vortexing of the samples, chloroform was added (1:5 chloroform:Trizol), followed by 5 seconds of vortexing and 2-3 minutes of incubation. The samples were then centrifuged at 12000 × g at 4 °C for 15 minutes. The upper, aqueous phase was isolated and 1.5 µl glycogen and 250 µl propanol was added. After vortexing, the samples were incubated at -20 °C overnight. The next day, the samples were centrifuged for 40 minutes at 12000 × g at 4 °C. The supernatant was discarded, and the RNA pellet was washed with freshly made, cold 75% ethanol. The samples were centrifuged again for 10 minutes at 7500 × g at 4 °C, and the ethanol wash step was repeated one more time. To dry out the pellet, the ethanol was discarded and the tubes left to air dry on ice. RNase free water was added, the samples were vortexed and then incubated for 10 minutes at room temperature. Samples were stored in -70 °C until DNase treatment.

Samples were DNase treated and re-purified using the GeneJET RNA Purification Micro Column kit (Thermo Scientific, K0842). The DNase mastermix was added directly into the tube with 30 µl extracted RNA and RNase free water solution made during RNA extraction. Through error, a deviation from the protocol occurred; 100 µl ethanol (100%) was added to the reaction mixture instead of 300 µl. The elution volume was increased to 22 µl nuclease free water.

Quality and quantity of extraction were analysed before purification using 1% agarose gel electrophoresis (90 V, 40 min) (Supplementary Figure S1) and Nanodrop, as well as after purification using Nanodrop (Supplementary Table S1). Plates with qPCR products were stored at room temperature until gel electrophoresis in disagreement with manufacturer's recommendations which might have caused some degradation by uracil-DNA glycosylase, which becomes active below 55 °C (Thermo Scientific, K0393). RNA concentration after

DNase purification was remeasured using the Qubit RNA Broad Range assay.

Reverse-transcription quantitative PCR (RT-qPCR)
cDNA synthesis was performed using the RevertAid First Strand cDNA Synthesis kit (Thermo Scientific, K1622), according to the manufacturer's protocol. Oligo (dT)18 primers, provided by the kit, were used to specifically target mRNA.

Primers targeting *Dachsous*, *E75*, *E74*, *Fat* and *Yorkie* transcripts were designed using Geneious Prime 2023.2.1 (https://www.geneious.com) based on in-house *Gerris buenoi* transcriptome and genome data. They were BLASTed and confirmed with the genome flat file on GenBank (GCA_001010745.2). Exon-exon spanning primers were designed using a preferred melting temperature (T_m) of 60 °C (58-62 °C), product length of 100 base pairs (bp) and primer length of 20 bp. Primer sequences can be found in Supplementary Table S2. Designed primers were ordered from Eurofins Genomics.

Dilution series of cDNA obtained from 12:12 and 18:6 female instar 5 (Day 2) were made. Five different concentrations (1.36 ng/µl, 0.272 ng/µl, 0.136 ng/µl, 0.0272 ng/µl, 0.0136 ng/µl) were used for qPCR to calculate primer efficiency for each primer pair. Three technical replicates were done for each sample, concentration and primer pair.

Reaction reagents for the quantitative PCR (qPCR), including the Hot Start Taq DNA polymerase, were provided by the Luminaris Color HiGreen qPCR Master Mix kit (Thermo Scientific, K0393). 20 µl reactions with 1 µl of template DNA were carried out with a final primer concentration of 0.3 µM and 2.5 mM $MgCl_2$. Non-template controls with nuclease free water instead of template were used to detect false positives due to reagent contamination and non-specific amplification. Reverse-transcriptase minus (RT-) controls which assess for DNA contamination in RNA samples were not run.

qPCR was carried out using SYBR Green and the Bio-Rad CFX96 Real-Time System together with the C1000 Touch Thermal cycler. A three-step cycling protocol was used; initial denaturation for 10 min at 95 °C, followed by 40 cycles of denaturation (95 °C for 15 s), annealing (60 °C for 30 s) and extension (72 °C for 30 s). An additional step was added to the cycling protocol (increase of temperature from 65 °C to 95 °C, increment 0.5 °C for 5 s) to obtain melting curves for validation of qPCR products. qPCR products were also validated using 1% agarose gel electrophoresis, as well as Sanger sequencing. Sanger sequencing results were analysed using BioEdit ver7.2.5 (Hall 1999) and visualised using Clustal Omega multiple sequence alignment program (Madeira *et al.* 2022).

RT-qPCR data analysis and statistics
Quantification cycle numbers (C_q) for each sample, concentration, primer pair and technical replicate were obtained using the CFX Manager software (Bio-Rad). Replicate groups of only one replicate and an obvious outlier C_q value were excluded in data analysis. To calibrate qPCR plates, the mean C_q value of five technical replicate reactions present on all plates (12:12 sample, 0.272 ng/µl, EFa primer pair) of one plate were used to normalise the C_q values of the other plates.

C_q value outliers were determined using Cook's distance. To calculate the primer efficiency (E), the quantification cycle number (C_q) was plotted against the sample concentration on logarithm base 10 scale. The slope was determined and then used in the following equation (Bustin *et al.* 2009):

$$E = 10^{-1/slope} - 1$$

Primer efficiency of 100% is ideal but 90-110% is acceptable for further analysis. R^2 values should be >98.0 (Taylor *et al.* 2010).

Results

Effect of photoperiod and sex on wing morph determination

To test the effect of photoperiod on wing morph distribution, wing morphologies of adult individuals reared in 12:12 and 18:6 conditions were scored. The proportion of micropterous (Mi), macropterous (Ma) and mesopterous (Me) wing morphs were as expected in these photoperiods; the majority of individuals became Ma (98.2%, n=56) in 12:12 and Mi (90.8%, n=65) in 18:6 (Figure 1). Me individuals were also found in both photoperiods; one individual in 12:12 and three individuals in 18:6. Individuals were also reared in intermediate photoperiods 15:9 (n=295) and 15.30:8.30 (n=345), to find critical photoperiods with a ~50:50 distribution of Mi and Ma morphs. Compared to a previous study (Gudmunds *et al.* 2022), the proportion of Mi were higher than expected in both photoperiods; 73.6% Mi, 24.1% Ma and 2.4% Me in 15:9 and 83.8% Mi, 13.0% Ma and 0.1% Me in 15.30:8.30 (Figure 1). There was a significant difference in the proportion of long-winged (Ma) and short-winged (Mi and Me) individuals between all photoperiods, except between 15.30:8.30 and 18:6 photoperiods (χ^2=2.94; df=1; p=0.086) (p-values are summarised in Supplementary Table S3). Additionally, there was a significant difference in wing morph proportion between sexes in both 15:9 and 15.30:8.30. The proportion of macropterous individuals was higher among males in 15:9 as well as 15.30:8.30 compared to females (χ^2=24.27; df=1; p=8.4e-07 and χ^2=12.90; df=1; p=0.00033, respectively), although more prominently in 15:9 (Figure 1). These results indicate that the reaction norm of *G. buenoi* to daylength is different between males and females, consistent with previous results (see Discussion).

There was no significant difference in wing morph proportions between females reared in 15:9 and 15.30:8.30 (χ^2=3.50; df=1; p=0.062). In contrast, I found that there was a significant difference between males from the two different intermediate photoperiods (χ^2=10.03; df=1; p=0.0015) (Figure 1), suggesting that the male reaction norm account for most of the differences in wing morph frequency between the intermediate photoperiods and that males are more affected by this 30-minute shift in photoperiod.

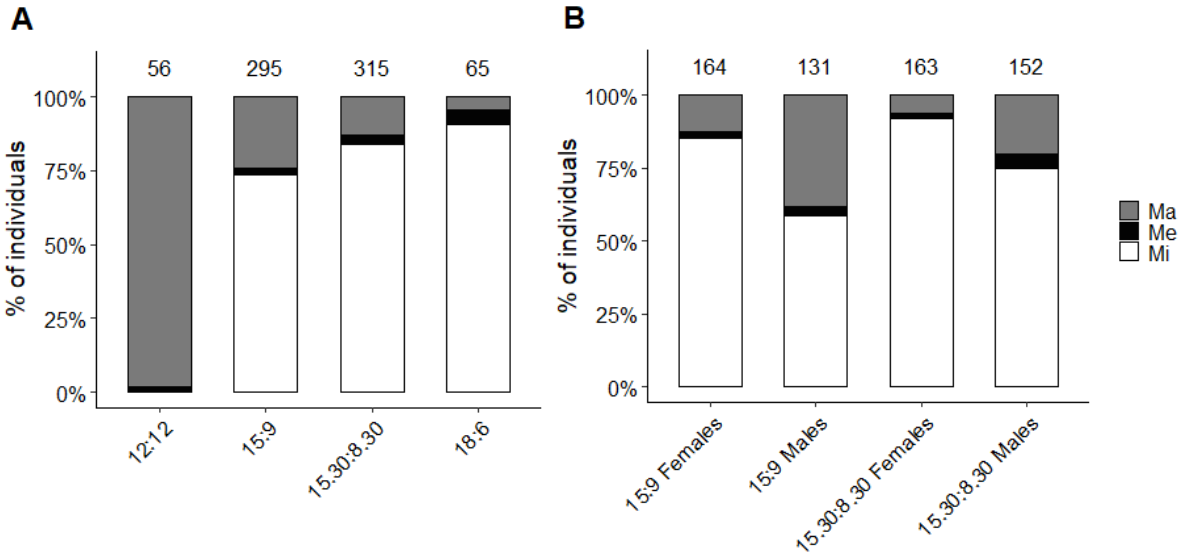

Figure 1: A) Proportion of individuals with macropterous (Ma), mesopterous (Me) and micropterous (Mi) wing morphs in 12:12, 15:9, 15.30:8.30 and 18:6 (hours light : hours dark) photoperiods. B) Proportion of individuals with macropterous (Ma), mesopterous (Me) and micropterous (Mi) wing morphs within each sex in intermediate photoperiods 15:9 and 15.30:8.30. Sample size for each photoperiod is indicated above the bars.

To examine the effect of photoperiod and sex on the difference in wing morph determination between 15:9 and 15.30:8.30 photoperiods, a generalised linear model (model 1) was constructed (for all generalised linear model parameters, see Supplementary Table S4). The statistical model showed that decreasing photoperiod had a significant negative effect on the probability that an individual emerge as short-winged (p=0.0012, b=-0.74; se=0.23), meaning that the probability of individuals acquiring long wings was higher in 15:9 photoperiod than in 15.30:8.30. Similarly, being male had a negative effect on becoming short-winged (p=5.4e-10; b=-1.4; se=0.23), i.e. there is a higher probability of a male becoming long-winged than a female in these photoperiods. According to this model, both photoperiod and sex independently have an effect on wing morph determination, although sex seems to have a greater effect in this experimental setting, where data is obtained from a small range of photoperiods.

When testing for an interaction between sex and photoperiod (model 2) I did not detect a significant interaction (p=0.99; b=-0.0037; se=0.47), indicating that males and females did not respond differently to the two photoperiods. The predicted probabilities from the interaction model are presented in Figure 2 and Supplementary Table S5.

Similar tests were done at the box level (model 3 and 4) using sex ratio and photoperiod as predictors of wing morph proportion. Due to singular fit issues, photoperiod and sex ratio were examined separately as predictors (model 5 and 6) (Supplementary Table S4). At this level, decreasing photoperiod had a significant negative effect on the proportion of short-winged individuals in a box (p=0.0043; b=-0.63; se=0.22) and being male did not (p=0.26; b=-1.1; se=0.96).

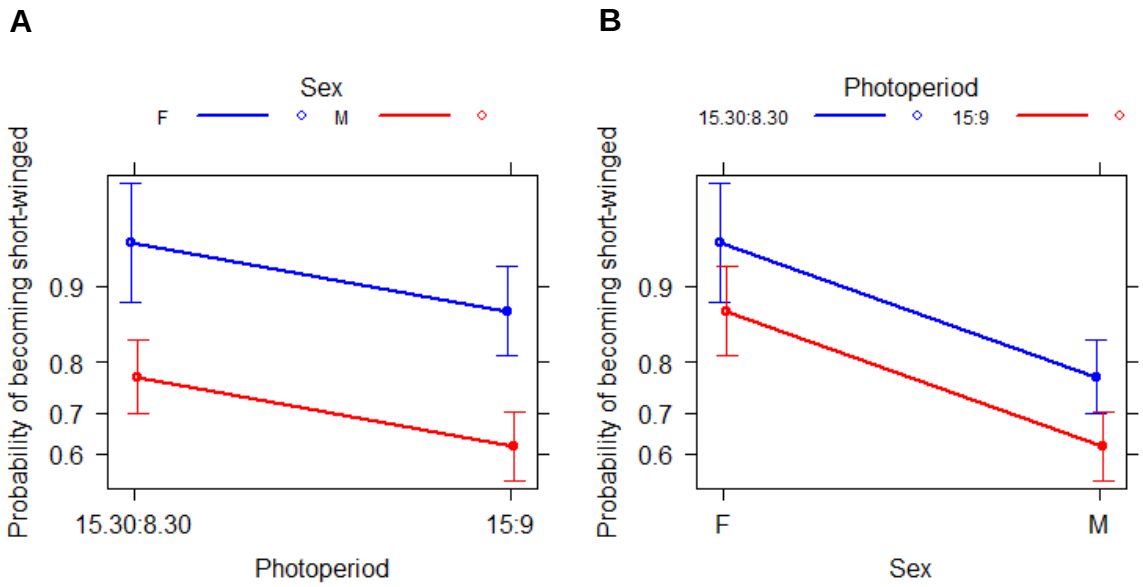

Figure 2: The effects of A) intermediate photoperiods (15.30:8.30 and 15:9) and B) sex (F, female; M, male) on wing morph determination on individual level. Y-axis represents the probability of becoming short-winged (micropterous or mesopterous), predicted by generalised linear modelling (model 2, see Supplementary Table S4). There is no interaction between the predictors (p=0.99; b=-0.0037; se=0.47). Sex has a greater effect on wing morph determination than photoperiod (p=9.7e-05; b=-1.4; se=0.37 and p=0.064; b=-0.74; se=0.40, respectively). Error bars represent 95% confidence intervals.

RT-qPCR product validation

Reverse-transcription quantitative PCR (RT-qPCR) was performed on transcripts of Fat, Ds, Yki, E74, E75 and EcR as well as the reference genes RPL9, EFa and RPS26. The transcripts were targeted using exon-exon junction spanning primers based on in-house *G. buenoi* transcriptome and genome data (primer sequences can be found in Supplementary Table S2). These target genes are of interest because of their implication in wing morph determination from recent studies in *G. buenoi* (Gudmunds 2023). The obtained qPCR products were validated based on melt curve analysis (Figure 3), gel electrophoresis (Figure 4), and Sanger sequencing (Supplementary Figure S2).

Melt curve analysis of qPCR products showed that every reaction product of the same primer pair had peaks at the same melting temperature (+/- 0.5 °C), indicating successful amplification of one singular product and the absence of byproducts (Figure 3 and Supplementary Table S6). This was true for all targets except EFa, which showed deviant melting peaks (Figure 3). There were peaks at ~78 °C in the EFa non-template controls (NTCs) suggesting that EFa product had been formed in this negative control as the result of contamination. Deviant melting temperatures at ~69-70 °C from EFa NTC 1, EFa NTC 2, EFa NTC 4 and EFa 18:6 low cDNA concentration (0.0136 ng/µl) reaction as well as ~74 °C in NTC 3 suggested byproducts smaller than the qPCR products, perhaps primer dimers. Other non-specific amplicons of higher melting temperature seemed to be present, as indicated by deviant melting peaks at ~81 °C from EFa NTC 4 and EFa 12:12 low cDNA concentration (0.0136 ng/µl) reaction (Figure 3).

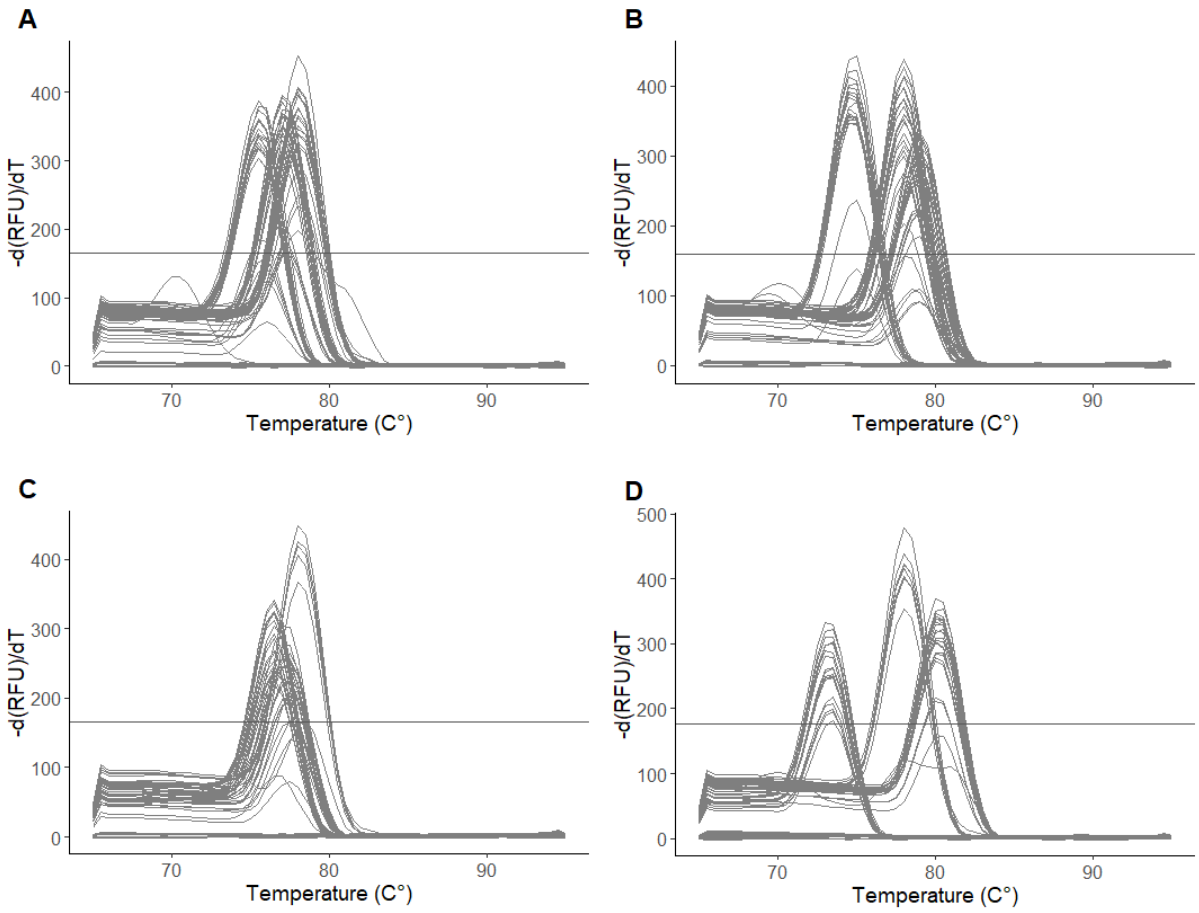
A
B
C
D
-d(RFU)/dT
Temperature (C°)
0
100
200
300
400
500
70
80
90

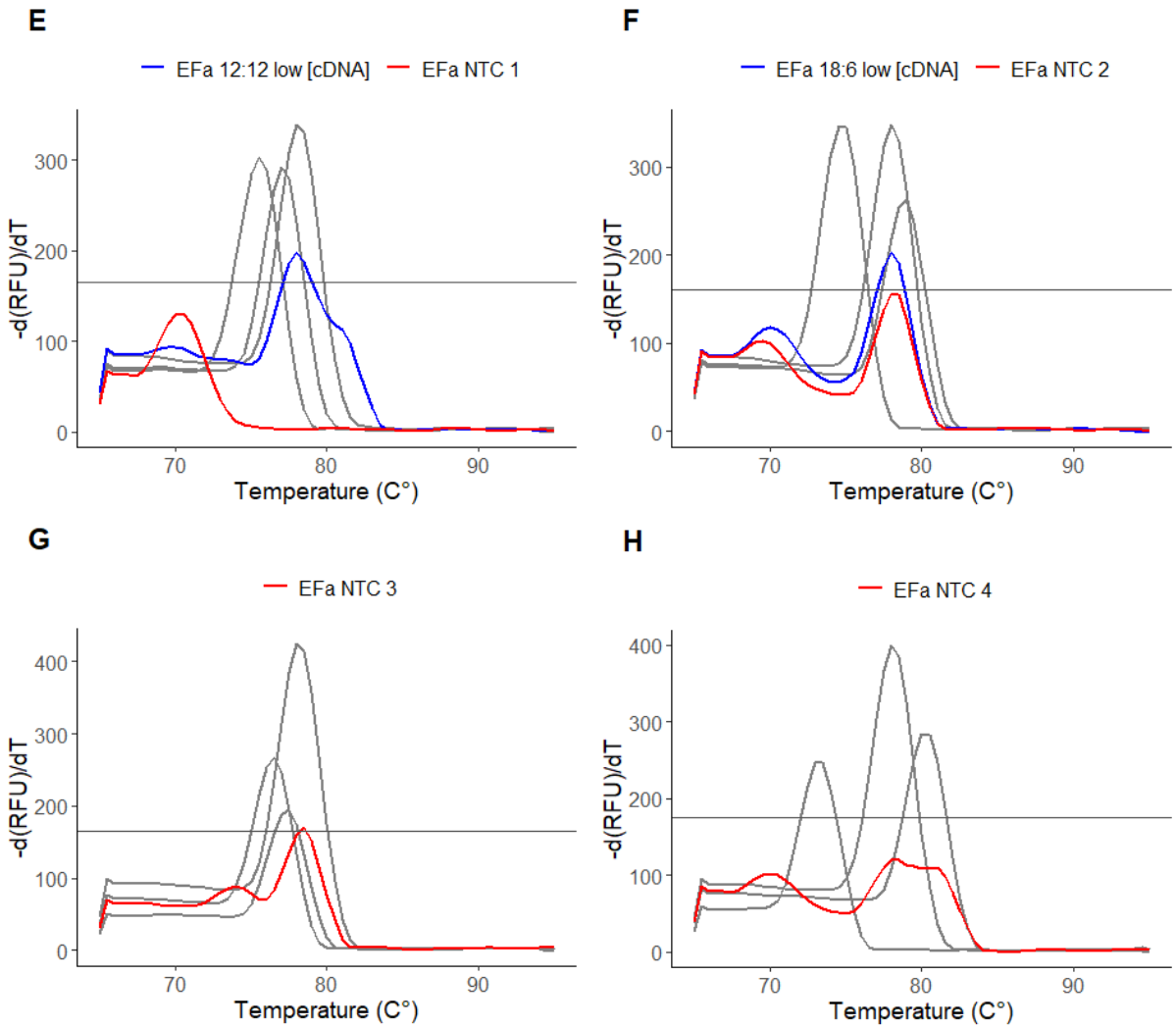

Figure 3: A-D) Melt peaks of qPCR products. Targeting transcripts of A) Ft, Ds and EFa, B) Yki, E74 and EFa, C) RPL9, RPS26 and EFa and D) EcR, E75 and EFa. E-H) Deviant melt peaks of qPCR products. E) Deviant melt peaks of EFa non-template negative control (EFa NTC 1) at ~70 °C and EFa 12:12 low cDNA concentration (0.0136 ng/µl) reaction at ~81 °C, along with expected peaks of Ft (75.50 C), Ds (77.00 °C), EFa (78.00 °C). F) Deviant melt peaks of EFa non-template negative control (EFa NTC 2) and EFa 18:6 low cDNA concentration (0.0136 ng/µl) reaction at ~69-70 °C, along with expected peaks of Yki (74.50 °C), E74 (79.00 °C), EFa (78.00 °C). G) Deviant melt peaks of EFa non-template negative control (EFa NTC 3) at ~74 °C, along with expected peaks of RPL9 (77.50 °C), RPS26 (76.50 °C), and EFa (78.00 °C). H) Deviant melt peaks of EFa non-template negative control (EFa NTC 4) at ~70 °C and ~81 °C, along with expected peaks of EcR (73.50 °C), E75 (80.00 °C), and EFa (78.00 °C). The straight line indicates the detection limit.

Agarose gel electrophoresis of qPCR products showed clear bands less than 250 nucleotides (nts) in size in each primer pair and sample reaction, as expected, indicating successful amplification of mRNA targets (Figure 4). Primers were visible in these lanes and in negative controls, as slightly shorter polynucleotides, giving rise to less clear bands. However, there were also bands with faded appearance of larger sized products, which could have been primer dimers. This was supported by the absence of E75 and EFa melt peaks in the E75 NTC and EFa NTC 1 reaction, respectively, and a melt peak at ~70 °C in the EFa NTC 1 reaction

(Figure 3). Contamination of EFa NTC 1, 3 and 4, as suggested by melting curve analysis, showed up as brighter bands at ~100 nt, similar to target products (Figure 4).

Unidentified artefacts also showed up in the gel. There was a band at ~250 nt (Figure 4), which could have given rise to the deviant 81 °C melt peak of EFa NTC 4 (Figure 3), since larger molecules generally have a higher melting temperature. Furthermore, there was a faded band at ~2000 nt across all lanes, indicating the presence of a large molecule in all reactions (Figure 4). It is not probable that this originated from contamination of qPCR reaction components since these components were not the same or were remade between plates. This may be DNA polymerase or uracil-DNA glycosylase, which was added in the qPCR reaction, binding to remaining DNA templates.

The Sanger sequencing results were aligned with target transcripts to examine whether the target gene was correctly amplified (Supplementary Figure S2). At least 30 nt long identical sequences of each sequencing product could be aligned with certainty to its corresponding target transcript, indicating that the target transcripts were successfully amplified during qPCR.

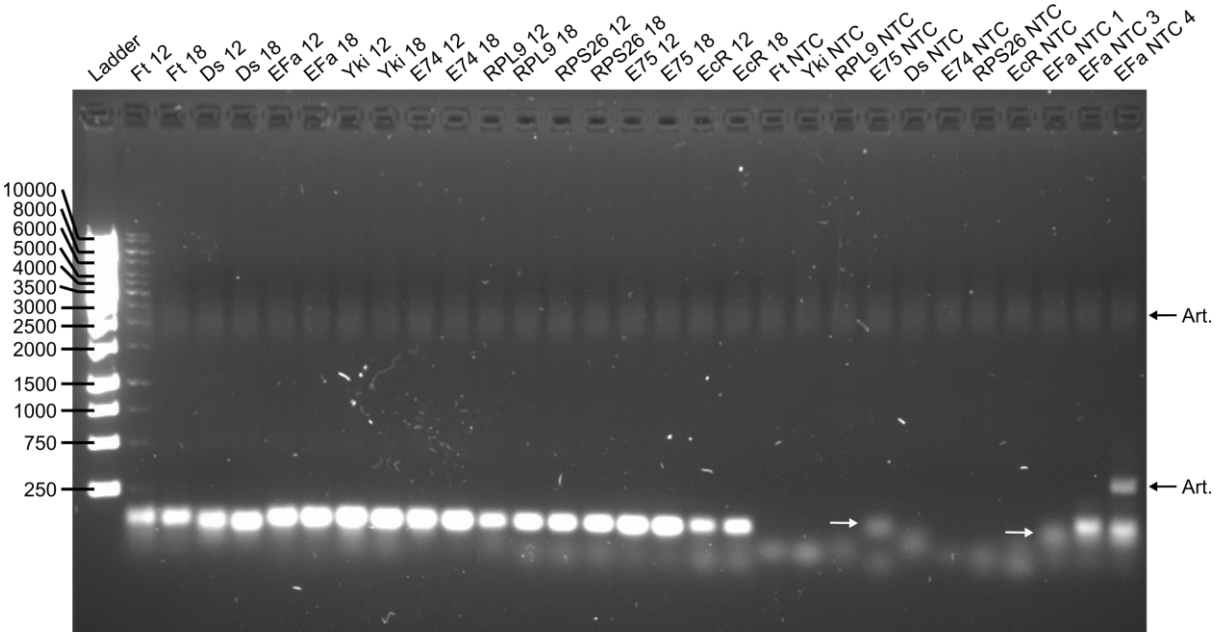

Figure 4: RT-qPCR product validation by gel electrophoresis. One reaction of each primer pair and sample were loaded (lane 1-18), along with non-template negative controls for every primer pair (lane 19-27) and extra EFa non-template negative controls of interest (lane 28-30). White arrows indicate possible primer dimers. Abbreviations: Ft, Fat; Ds, Dachsous; Yki, Yorkie; NTC, non-template control; Art., unknown artefact.

C_q range and primer efficiency

To find the optimal range of cDNA concentration input in qPCR reactions with Ft, Ds, EFa, Yki, E74, E75, EcR, RPL9 and RPS26 transcripts as targets, five cDNA concentrations of each sample (12:12 and 18:6) were used in the qPCR. This was done to create standard curves, from which primer efficiencies could be calculated and stability of reference genes across photoperiod conditions could be evaluated (Figure 5). All the obtained C_q values ranged between ~24-39 cycles. The EFa reactions had a noticeable lower range (24-35 cycles), which indicated that EFa mRNA was more expressed compared to mRNA of the

other genes. A higher variance among technical replicates and loss of replicates due to the fluorescence signal being below the detection limit were observed in the qPCR reactions containing the two lowest cDNA concentrations (0.0272 ng/µl and 0.0136 ng/ µl). These observations indicate an approximate lower limit of viable cDNA input concentrations for all genes except EFa, and C_q values obtained in this range (>36) should be used with caution.

The two lowest concentrations or the lowest concentration were removed from models to improve linearity, and the standard curves with the improved R^2 values are found in Figure 5. Reactions with an R^2 value within the acceptable range (>0.98) (Taylor *et al.* 2010) include the Ft reaction with the 12:12 sample and the Ds, Yki and E75 reactions with the 18:6 sample. Adequate primer efficiency (90-110%) (Taylor *et al.* 2010) was obtained when E74 and E75 were targeted in the 12:12 sample. However, the only reaction which fulfilled both requirements for quantification analysis was the EFa reaction with the 12:12 sample.

High variance was seen in replicate groups of higher concentrations as well, with some reaching up to a >1 cycle difference (Figure 5). The amplification efficiency of primer pairs varied between photoperiods in many cases, as visualised by the varying slopes in each graph in Figure 5. Importantly, three out of four EFa NTCs had positive results (EFa NTC 2: C_q=36.34; EFa NTC 3: C_q=35.63; EFa NTC 4: C_q=35.05), which could be attributed to contamination as indicated by melt curve analysis and gel electrophoresis of products (Figure 3 and 4).

Across almost all concentrations and primers, the 18:6 sample had lower C_q values, indicating decreased expression of target genes in the 18:6 treatment (Figure 5). Since primer efficiencies were not within the desired range for further expression analysis, this could not be investigated. However, the consistently lower C_q values of 18:6 could also be explained by less cDNA starting material resulting from lower cDNA concentration in the 18:6 samples than assumed (see Discussion). This trend of lower C_q values in the 18:6 sample compared to the 12:12 sample was also seen in the reference gene RPS26, potentially indicating low stability across photoperiod treatments. For reactions of the reference gene RPL9 and EFa, the trend was not as clear. High variance in C_q between technical replicates in RPL9 reactions and inadequate R^2 and slope values prevented any conclusions about the stability of the reference genes (Figure 5).

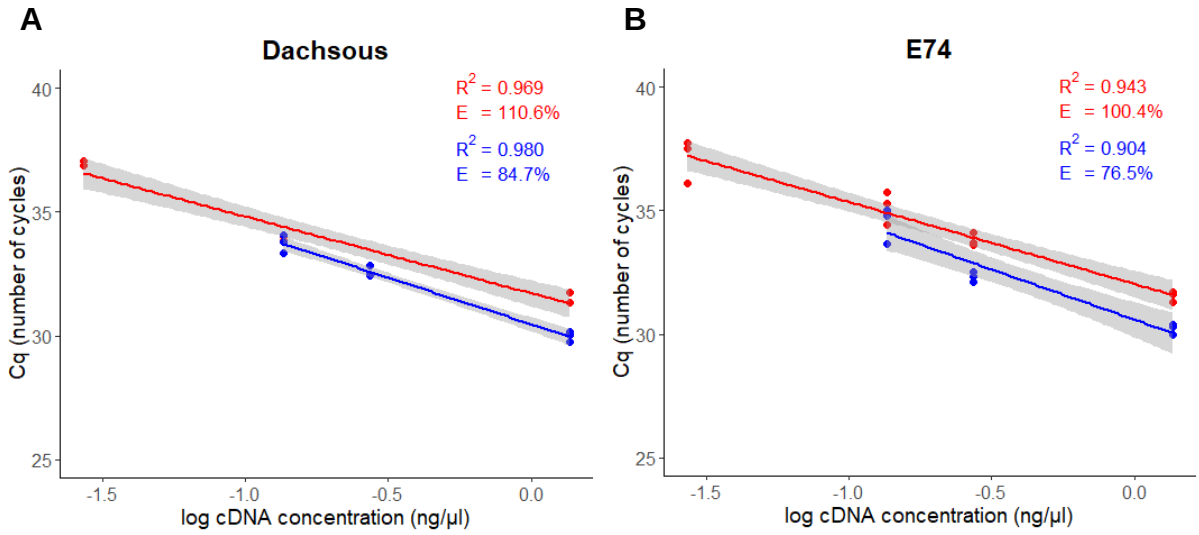

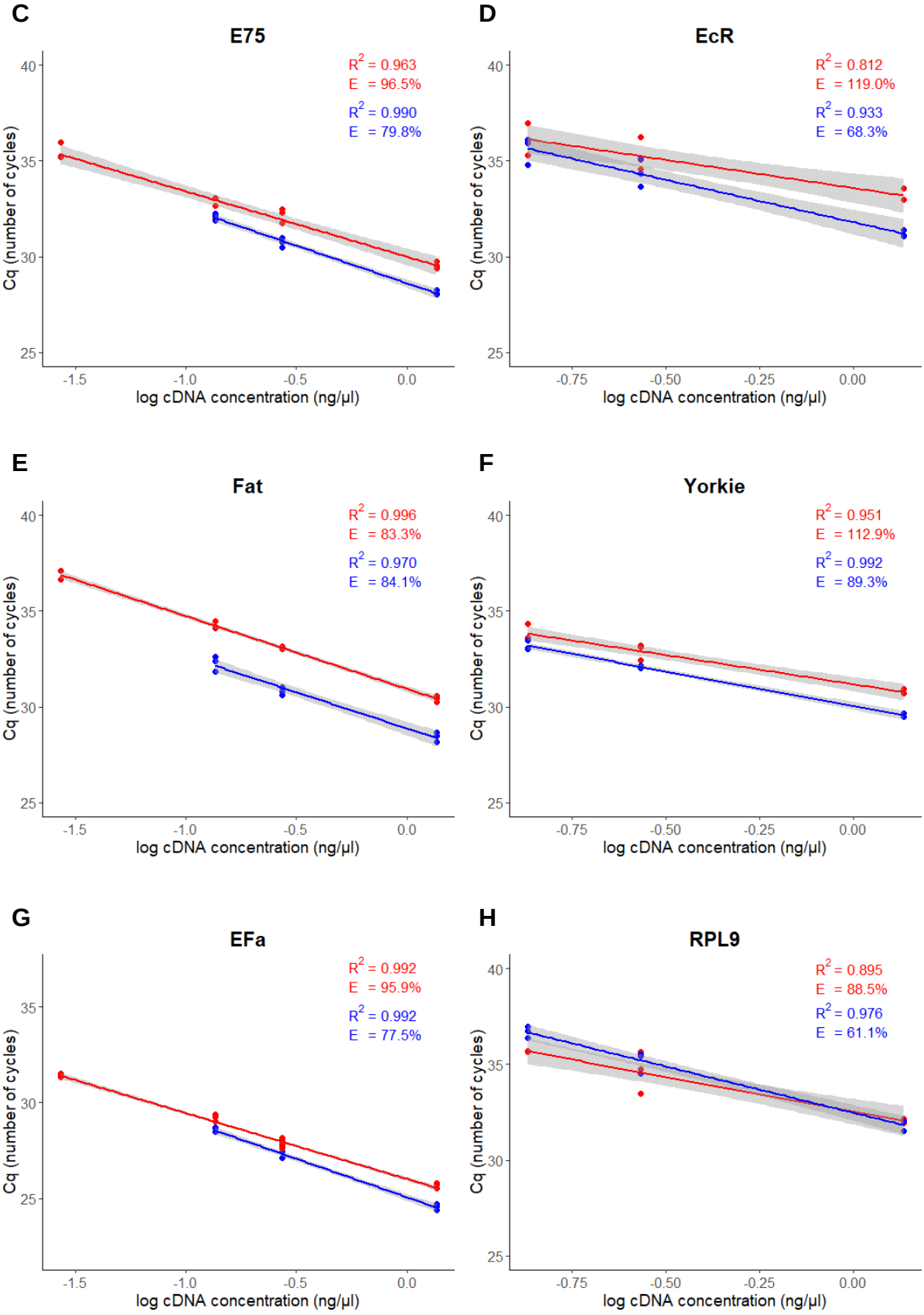
C
E75
R2 = 0.963
E = 96.5%
R2 = 0.990
E = 79.8%
Cq (number of cycles)
log cDNA concentration (ng/µl)
D
EcR
R2 = 0.812
E = 119.0%
R2 = 0.933
E = 68.3%
Cq (number of cycles)
log cDNA concentration (ng/µl)
E
Fat
R2 = 0.996
E = 83.3%
R2 = 0.970
E = 84.1%
Cq (number of cycles)
log cDNA concentration (ng/µl)
F
Yorkie
R2 = 0.951
E = 112.9%
R2 = 0.992
E = 89.3%
Cq (number of cycles)
log cDNA concentration (ng/µl)
G
EFa
R2 = 0.992
E = 95.9%
R2 = 0.992
E = 77.5%
Cq (number of cycles)
log cDNA concentration (ng/µl)
H
RPL9
R2 = 0.895
E = 88.5%
R2 = 0.976
E = 61.1%
Cq (number of cycles)
log cDNA concentration (ng/µl)

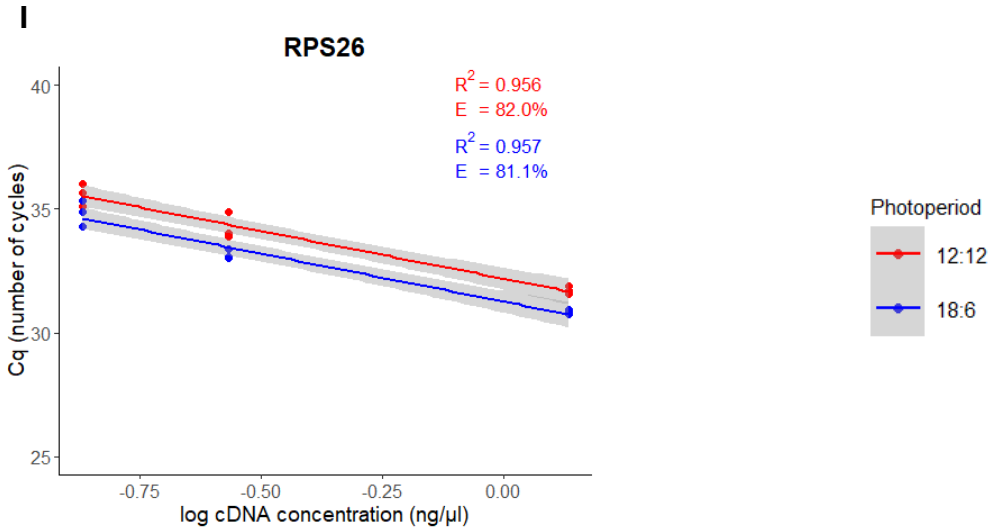

Figure 5: Standard curves obtained from qPCR reactions with wing-tissue sampled from striders reared in 12:12 and 18:6, respectively, and primer pairs for each gene target. The gene targets were A) Dachsous, B) E74, C) E75, D) EcR, E) Fat, F) Yorkie, G) EFa, H) RPL9 and I) RPS26. Primer efficiency E is derived from the slope of the standard curves. The shadowed region represents a 95% confidence interval. Regression model parameters can be found in Supplementary Table S7.

Discussion

In this study, the proportion of photoperiodically induced wing morphs in the water strider *Gerris buenoi* was investigated and an RT-qPCR protocol for *G. buenoi* wing tissue was developed for assaying the expression of novel genes. This was done to enable future experiments investigating the molecular mechanism of wing morph determination. Results from *G. buenoi* studies have shown that the hormone ecdysone and the Hippo pathway are involved (Gudmunds 2023). Ecdysone probably integrates photoperiodic information and the signal is then transduced to the Fat/Hippo pathway which regulates wing development. Further studies are needed to fully elucidate this putative mechanism.

Dynamics of periodically induced wing polyphenism in *G. buenoi*

The proportion of wing morphs was determined in both extreme (12:12 and 18:6) and intermediate (15.30:8.30 and 15:9) photoperiods. As previously described (Gudmunds *et al.* 2022), the 12:12 photoperiod resulted in an absolute majority of macropterous (Ma) individuals, and the 18:6 resulted in a majority of micropterous (Mi) individuals (Figure 1).

The wing morph frequencies in intermediate photoperiods observed in this study were not as expected, with a majority of Mi individuals in both 15.30:8.30 (74% Mi) and 15:9 (84% Mi) (Figure 1). This is not in line with earlier studies in the same lab in which the Ma individuals made up the majority (Gudmunds *et al.* 2022). There is no clear explanation for this difference. Rearing density can affect wing morph distribution, with higher density leading to more Ma individuals (Gudmunds *et al.* 2022). However, despite higher rearing density compared to the study by Gudmunds *et al*. (2022), the proportion of Ma individuals was lower in this study. One possibility is that around the particular photoperiod studied, other environmental factors have additional impact on shifts in frequencies and/or that the striders are more sensitive to variation in density and therefore even small variation in density have a

disproportionate effect on wing morph proportions. It is likely that, even though photoperiod evidently is the major environmental cue that determines wing morph in *G. buenoi* (Gudmunds *et al.* 2022), that other environmental factors like variation in nutrition or temperature can have an effect in these conditions. More studies are needed to explore how other environmental factors and/or cues interact to regulate wing polyphenism in *G. buenoi*.

The results from the photoperiod experiments show that only a 30-minute shift in photoperiod can significantly affect the proportion of wing morphs; 15.30:8.30 had a higher percentage of Mi individuals compared to 15:9, in line with the notion that more hours of daylight result in more short-winged individuals (Gudmunds *et al.* 2022) (Figure 1). Interestingly, the proportion of the Ma morph was higher among males than females, indicating a sex-biased effect of photoperiod (Figure 1). Previous studies have also shown this (Spence 1989, Gudmunds *et al.* 2022, Zera & Denno 1997). This sex-biased effect has also been observed when looking at density-dependent wing morph induction in *G. buenoi* (Gudmunds *et al.* 2022) and another water strider (Han 2020). This could be explained by the trade-off between reproduction and dispersal; it takes energy for a female to produce eggs, and since this cost does not apply to males, it is more favourable for males to develop wings. There are advantages to having wings, such as being able to move away from a habitat with depleted resources when population size increases (Roff 1986, Zera & Denno 1997). It has been observed that 18:6 nymphs destined to have short wings have shorter developmental time than 12:12 nymphs (Gudmunds 2023). There might be an advantage for the sexes to emerge at different times, potentially driving this coupling of wing length and developmental time. For example, it could be favourable for females to emerge earlier than males to avoid harassment and males could more easily find mating partners if they disperse later than females.

While there was an overall strong effect of both photoperiod and sex on wing morph determination, I could not detect a significant interaction between the two (Figure 2 and Supplementary Table S4). Thus, the sex difference observed in the intermediate photoperiods was not large enough for it to be statistically significant. When analysed at the box level, photoperiod had significant effect on wing morph proportion, and sex ratio did not (Supplementary Table S4). This is likely due to the limitations in the experimental design, like low variation in sex ratio between boxes.

Validation of RT-qPCR protocol for wing-tissue

The existing RT-qPCR method for gene expression analysis of Ft, Ds, Yki, EcR, E75 and E74 transcripts in *G. buenoi* wing-buds were validated and expanded. One RNA sample from presumably long-winged individuals reared in 12:12 and one from presumably short-winged individuals reared in 18:6 was used to synthesise cDNA for the qPCR reaction. Amplification products were analysed using melt curves, gel electrophoresis as well as sequencing, and standard curves were made to evaluate primer efficiency. Quantification of mRNA levels of these genes were not done, firstly because of the inadequate quality of the data (discussed more below), and secondly because of the lack of biological replicates. Even if the data allowed for quantification, the results would not have biological significance.

Validation of qPCR products indicated that the targets were amplified and melt curves indicated that one singular product of one melting point was amplified, in most reactions (Figure 3). Alignment of sequencing products and target sequences confirmed the presence of target sequences in qPCR reactions (Supplementary Figure S2). Sequence identity of stretches of at least 30 nt was estimated to be an adequate measure, however this cut-off is arbitrary and based on common sense. Gel electrophoresis further supported successful target

amplification, showing bands of the expected product length of 100 nt (<250 nt according to ladder) (Figure 4).

Even though targets were indeed amplified, the RT-qPCR results could not be used for quantification. Primer efficiencies were mostly outside the acceptable range (90-110%) (Taylor *et al.* 2010), which could be a result of many faults in the RT-qPCR protocol including inadequate primer design, reaction conditions, cDNA sample quality, reagent concentrations and presence of inhibitors (Bustin & Nolan 2004, Bustin *et al.* 2009, Taylor *et al.* 2010, Schrader *et al.* 2012). Gel electrophoresis and melt curves analysis of qPCR products indicated that there are non-specific products present and contaminated samples, especially in the EFa reactions with no added template (NTCs) and low template concentration (Figure 3 and 4). The artefacts with lower melting point than the target sequence could be attributed to primer dimers. The amplification of EFa target sequence in EFa NTCs 2-4 as indicated by 78 °C melt peaks, bands of the expected product length in the gel and positive qPCR reactions indicated contamination of these reactions. Because no such contamination was seen in other NTCs, I concluded that either the forward or reverse EFa stock primer solution had been contaminated. Hence, the results of the EFa RT-qPCR assay could not be trusted. Non-specific amplicons such as primer dimers affect primer efficiency and could lead to false quantification (Bustin *et al.* 2009). However, the high concentration samples did not show the presence of primer dimers, suggesting that primer dimers should not affect amplification of target markedly in these cases. Nonetheless, my advice would be to design new EFa primers in future studies.

Other unknown artefacts were also detected in melt curve analysis and gel electrophoresis, some in both and some in either of the analysis methods. It could have been non-specific amplicons, primer dimers or contamination. I hypothesised that the faded band at ~2000 nt across all lanes were DNA polymerase or uracil-DNA glycosylase binding to DNA template. Plates with qPCR products were stored at room temperature until gel electrophoresis in disagreement with manufacturer's recommendations which might have caused some degradation by uracil-DNA glycosylase, which becomes active again below 55 °C (Thermo Scientific, K0393).

Too low concentration of cDNA samples could be a reason for skewed primer efficiencies and linearity (Karrer *et al.* 1995, Bustin & Nolan 2004, Bustin *et al.* 2009). The results indicated that the concentrations used were not within the dynamic linear range, since R^2 values were too low (≤0.98) (Taylor *et al.* 2010). The solution for this could be to use a higher range of concentrations to obtain C_q values at the exponential phase and consequently get C_q values that better fit the linear regression model. Results indicate that a cut-off point of reliable C_q values was reached at a cDNA concentration of around 0.0272 ng/ µl (for most genes, see Results). From that point, the variance within technical replicates increased and some replicates were lost (Figure 5). However, it is possible that the theoretical starting cDNA concentrations were off which would mean that the analysis of the acceptable cDNA concentration range is inaccurate. The RNA concentration was measured about two weeks before the corresponding cDNA was diluted, and sample degradation could have happened during this time. Ideally, the cDNA concentration should have been measured again closer to performing the qPCR to verify the final cDNA concentrations used in qPCR reactions. There was a clear trend of lower C_q values of the 18:6 sample across all concentrations compared to the 12:12 sample, which could mean that these genes have increased expression in this photoperiod (cannot be confirmed by these data), or that the 18:6 cDNA input concentration was lower than the theoretical concentration due to RNA or cDNA degradation.

Another potentially important problem was the sample purity. Nanodrop measurements (Supplementary Table S1) of RNA samples after purification and DNAse treatment indicated a presence of organic compounds, likely phenol or glycogen (Matlock 2015) which originates from the RNA extraction. Both are PCR inhibitors (Schrader *et al.* 2012), and their presence in qPCR reactions can lead to decreased primer efficiency (Bustin *et al.* 2009).

Limitations of this study also include the absence of controls recommended by the cDNA synthesis kit and qPCR kit manufacturer (Thermo Scientific, K1622 and K0393, respectively) and literature (Bustin *et al.* 2009), which would have aided in the troubleshooting. Reverse-transcriptase minus (RT-) negative controls would have controlled for the presence of genomic DNA contamination and off-target amplification in RNA samples. Dilution series of positive controls such as GAPDH control RNA and known *G. buenoi* RNA would have helped in determining if PCR inhibitors are lowering the amplification efficiency.

Overall, the RT-qPCR experiments presented in this study had several major limitations. Because of inadequate RNA purity, inconsistencies in primer efficiency probably due to PCR inhibitors and non-specific amplification, high variance in C_q within technical replicate groups and lack of data points of higher sample cDNA concentrations, the results from the qPCR were not conclusive. Before future qPCR gene expression analysis, I would advise to redo this experiment with new EFa primers and higher cDNA concentrations for the other gene targets. This will aid in finding the appropriate range of cDNA input and properly evaluating primer design and reference gene stability.

Conclusions and future studies

The data presented in this thesis demonstrated that *G. buenoi* reared in intermediate photoperiods 15.30:8.30 and 15:9 resulted in a majority of Mi individuals and that the response to photoperiod was sex-biased, with males more likely to become Ma. This suggests that the critical photoperiod, giving rise to an about 50:50 distribution of Ma and Mi individuals, is a photoperiod with shorter daylight. At the molecular level, I find that the current protocol for RT-qPCR of wing-tissue to investigate expression of *Ft*, *Ds*, *Yki*, *E74*, *E75* and *EcR* with the use of *RPL9*, *RPS26* and *EFa* as reference genes need further validation. In particular, the protocol should be repeated with higher cDNA input. All primer pairs did target and amplify the target sequences, but gel electrophoresis and melt curve analysis indicated that EFa primers produced non-specific amplification which lower amplification efficiency.

Despite the clear limitations, this study provides insight into how to design future functional genetic studies of wing polyphenism in *G. buenoi*. By determining the expression of these genes and further investigating the dynamics of the wing morph response to photoperiods in *G. buenoi*, we will better understand the molecular mechanism behind wing polyphenism in insects, how environmental cues can induce phenotypic plasticity and how this has evolved.

Acknowledgements

I am grateful to Arild Husby for letting me do my master thesis in his research group, and I would like to thank both him and Erik Gudmunds for their supervision. Your guidance and feedback have been invaluable. I would also like to thank McKenna Burns for all your help and encouragement during this project. Finally, thanks to Aleix Palahí Torres for being a helpful hand during strider rearing.

References

Andersen NM. 1993. The Evolution of Wing Polymorphism in Water Striders (Gerridae): A Phylogenetic Approach. Oikos 67: 433–443.

Biassoni R, Raso A (eds). 2014. Quantitative Real-Time PCR: Methods and Protocols. 1st ed. Springer New York, New York, NY. doi 10.1007/978-1-4939-0733-5.

Biomatters. 2023.2.1. Geneious Prime. Auckland, New Zealand. URL: https://www.geneious.com.

Bustin SA, Benes V, Garson JA, Hellemans J, Huggett J, Kubista M, Mueller R, Nolan T, Pfaffl MW, Shipley GL, Vandesompele J, Wittwer CT. 2009. The MIQE Guidelines: Minimum Information for Publication of Quantitative Real-Time PCR Experiments. Clinical Chemistry 55: 611–622.

Bustin SA, Nolan T. 2004. Pitfalls of Quantitative Real-Time Reverse-Transcription Polymerase Chain Reaction. Journal of Biomolecular Techniques : JBT 15: 155–166.

Fairbairn DJ, King E. 2009. Why do Californian striders fly? Journal of Evolutionary Biology 22: 36–49.

Fawcett MM, Parks MC, Tibbetts AE, Swart JS, Richards EM, Vanegas JC, Cenzer M, Crowley L, Simmons WR, Hou WS, Angelini DR. 2018. Manipulation of insulin signaling phenocopies evolution of a host-associated polyphenism. Nature Communications 9: 1699.

Gotoh H, Hust JA, Miura T, Niimi T, Emlen DJ, Lavine LC. 2015. The Fat/Hippo signaling pathway links within-disc morphogen patterning to whole-animal signals during phenotypically plastic growth in insects. Developmental Dynamics 244: 1039–1045.

Gudmunds E. 2023. From environmental cue to phenotypic variation – a functional investigation of wing polyphenism in an emerging model species. PhD dissertation, Acta Universitatis Upsaliensis, Uppsala.

Gudmunds E, Narayanan S, Lachivier E, Duchemin M, Khila A, Husby A. 2022. Photoperiod controls wing polyphenism in a water strider independently of insulin receptor signalling. Proceedings of the Royal Society B: Biological Sciences 289: 20212764.

Hall, TA. 1999. BioEdit: a user-friendly biological sequence alignment editor and analysis program for Windows 95/98/NT. Nucleic Acids Symposium Series 41: 95-98.

Han CS. 2020. Density-dependent sex-biased development of macroptery in a water strider. Ecology and Evolution 10: 9514–9521.

Harada T, Numata H. 1993. Two critical day lengths for the determination of wing forms and the induction of adult diapause in the water strider, Aquarius paludum. Naturwissenschaften 80: 430–432.

Higuchi R, Dollinger G, Walsh PS, Griffith R. 1992. Simultaneous amplification and

detection of specific DNA sequences. Bio/Technology (Nature Publishing Company) 10: 413–417.

Higuchi R, Fockler C, Dollinger G, Watson R. 1993. Kinetic PCR Analysis: Real-time Monitoring of DNA Amplification Reactions. Bio/Technology 11: 1026–1030.

Iwanaga K, Tojo S. 1986. Effects of juvenile hormone and rearing density on wing dimorphism and oöcyte development in the brown planthopper, Nilaparvata lugens. Journal of Insect Physiology 32: 585–590.

Karrer EE, Lincoln JE, Hogenhout S, Bennett AB, Bostock RM, Martineau B, Lucas WJ, Gilchrist DG, Alexander D. 1995. In situ Isolation of mRNA from Individual Plant Cells: Creation of Cell-Specific cDNA Libraries. Proceedings of the National Academy of Sciences of the United States of America 92: 3814–3818.

Lin X, Xu Y, Jiang J, Lavine M, Lavine LC. 2018. Host quality induces phenotypic plasticity in a wing polyphenic insect. Proceedings of the National Academy of Sciences 115: 7563–7568.

Madeira F, Pearce M, Tivey ARN, Basutkar P, Lee J, Edbali O, Madhusoodanan N, Kolesnikov A, Lopez R. 2022. Search and sequence analysis tools services from EMBL-EBI in 2022. Nucleic Acids Research 50: W276–W279.

Matlock B. 2015. Assessment of Nucleic Acid Purity. WWW document: https://assets.thermofisher.com/TFS-Assets/CAD/Product-Bulletins/TN52646-E-0215M-NucleicAcid.pdf. Accessed 12 September 2023.

Nijhout HF. 2003. Development and evolution of adaptive polyphenisms. Evolution & Development 5: 9–18.

Ririe KM, Rasmussen RP, Wittwer CT. 1997. Product Differentiation by Analysis of DNA Melting Curves during the Polymerase Chain Reaction. Analytical Biochemistry 245: 154–160.

Roff DA. 1986. The Evolution of Wing Dimorphism in Insects. Evolution 40: 1009–1020.

Roff DA. 1984. The Cost of Being Able to Fly: A Study of Wing Polymorphism in Two Species of Crickets. Oecologia 63: 30–37.

Schrader C, Schielke A, Ellerbroek L, Johne R. 2012. PCR inhibitors – occurrence, properties and removal. Journal of Applied Microbiology 113: 1014–1026.

Simpson SJ, Sword GA, Lo N. 2011. Polyphenism in Insects. Current Biology 21: R738–R749.

Spence JR. 1989. The habitat templet and life history strategies of pond skaters (Heteroptera: Gerridae): reproductive potential, phenology, and wing dimorphism. Canadian Journal of Zoology 67: 2432–2447.

Svec D, Tichopad A, Novosadova V, Pfaffl MW, Kubista M. 2015. How good is a PCR efficiency estimate: Recommendations for precise and robust qPCR efficiency assessments. Biomolecular Detection and Quantification 3: 9–16.

Taylor S, Wakem M, Dijkman G, Alsarraj M, Nguyen M. 2010. A practical approach to RT-qPCR—Publishing data that conform to the MIQE guidelines. Methods 50: S1–S5.

Vellichirammal NN, Gupta P, Hall TA, Brisson JA. 2017. Ecdysone signaling underlies the pea aphid transgenerational wing polyphenism. Proceedings of the National Academy of Sciences 114: 1419–1423.

Vellichirammal NN, Madayiputhiya N, Brisson JA. 2016. The genomewide transcriptional response underlying the pea aphid wing polyphenism. Molecular Ecology 25: 4146–4160.

Vepsäläinen K. 1971. The role of gradually changing daylength in determination of wing length, alary dimorphism and diapause in a Gerris odonlogaster (Zett.) population (Gerridae, Heteroptera) in South Finland. Annales Academiae Scientiarum Fennicae (Series A, IV Biologica) 183: 1–25.

Vepsäläinen K. 1974. Determination of wing length and diapause in water-striders (Gerris Fabr., Heteroptera). Hereditas 77: 163–175.

West-Eberhard MJ. 2003 Developmental plasticity and evolution. Oxford University Press, Oxford, UK.

Wittwer CT, Herrmann MG, Moss AA, Rasmussen RP. 1997. Continuous Fluorescence Monitoring of Rapid Cycle DNA Amplification. BioTechniques 22: 130–138.

Xu H-J, Xue J, Lu B, Zhang X-C, Zhuo J-C, He S-F, Ma X-F, Jiang Y-Q, Fan H-W, Xu J-Y, Ye Y-X, Pan P-L, Li Q, Bao Y-Y, Nijhout HF, Zhang C-X. 2015. Two insulin receptors determine alternative wing morphs in planthoppers. Nature 519: 464–467.

Zera AJ. 2003. The Endocrine Regulation of Wing Polymorphism in Insects: State of the Art, Recent Surprises, and Future Directions1. Integrative and Comparative Biology 43: 607–616.

Zera AJ, Denno RF. 1997. Physiology and ecology of dispersal polymorphism in insects. Annual Review of Entomology 1997 42: 207-230.

Zhang C-X, Brisson JA, Xu H-J. 2019. Molecular Mechanisms of Wing Polymorphism in Insects. Annual Review of Entomology 64: 297–314.

Supplementary materials

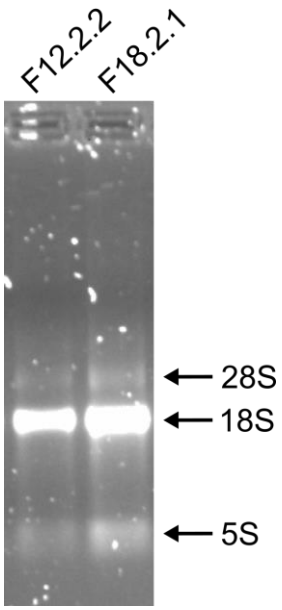

Figure S1: Gel electrophoresis RNA quality and quantity assessment of samples. This was done pre-column, before DNase treatment and re-purification. The RNA from wing buds of eight and five individuals from 12:12 (F12.2.2) and 18:6 (F18.2.1), respectively, were extracted. Arrows indicate the bands of 28S, 18S and 5S rRNA.

Table S1: Nanodrop and Qubit RNA concentration measurement and Nanodrop quality assessment.

Sample	Pre-purification Nanodrop conc. (ng/µl)	Post-purification Nanodrop conc. (ng/µl)	Post-purification Qubit conc. (ng/µl)[a]	260/280	260/230
F12.2.2	40.6	13.3	13.6	1.92	0.60
F18.2.1	68.7	34.1	37.4	2.05	1.41

[a] Used for calculation of dilution series.

Table S2: qPCR primer sequences.

Target	Forward	Reverse
Dachsous	TGACAATGTGCCACAGTTCC	GCTTGGACAGTCAAAAGGGC
E75	TTATGATGGCCAGGGACCAG	AACTCTTGCTGGCCAGTCAA
E74	ACTACCCTCAGCCACACCAT	GTGTAATAACCGCCCCCACC
EcR	GCTAAAAGATTACCCGGATTC	TTCGTGCCATTCTCAACATC
EFa	ATTCCACACACATAGGCTTG	CGTCGTACCGGTAAGACTAC
Fat	CGTCGTACCGGTAAGACTAC	ACTTGACCAGGCCTTTCAAGA
RPL9	GTTGACTGCTGGATAAGAGC	TTACGGTGACCAACTCTACC
RPS26	ACAGTAGTGAAGCTT	AGAAATATCGTTGAA
Yorkie	GAACAGGCTACGACCGCAG	GCCCTCTGCAGATGAACAGG

Table S3: χ2 test p-values for difference in wing morph proportions between photoperiods.

	12:12	15:9	15.30:8.30
15:9	< 2.2e-16 ***		
15.30:8.30	< 2.2e-16 ***	0.00063 **	
18:6	< 2.2e-16 ***	0.00083 **	0.086 NS

* $p < 0.05$, ** $p < 0.005$, *** $p < 0.0005$.

Table S4: Generalised linear model parameters.

Model number	Description	Fixed effects	Estimate	Std. error	z value	*p*
1	Generalised linear model with random effects (GLMER). Sex and photoperiod as independent predictors of wing morph. Boxes as random effect. Individual level.	Intercept	2.668	0.246	10.840	<2e-16 ***
		Photoperiod 15:9	-0.738	0.228	-3.232	0.00123 **
		Sex male	-1.439	0.232	-6.207	5.42e-10 ***
2	Generalised linear model with random effects (GLMER). Sex and photoperiod as independent predictors of wing morph and their interaction. Boxes as random effect. Individual level.	Intercept	2.667	0.324	8.231	<2e-16 ***
		Photoperiod 15:9	-0.735	0.397	-1.851	0.0642
		Sex male	-1.437	0.369	-3.900	9.68e-05 ***
		Photoperiod 15:9 : Sex male	-0.004	0.472	-0.008	0.994
3	Generalised linear model with random effects (GLMER). Sex ratio and photoperiod as independent predictors of wing morph proportion. Boxes as random effect. Box level.	Intercept	2.553	0.465	5.491	3.99e-08 ***
		Photoperiod 15:9	-0.700	0.214	-3.275	0.00106 **
		Sex ratio[a]	-1.566	0.862	-1.816	0.0693
4	Generalised linear model with random effects (GLMER). Sex ratio and photoperiod as independent predictors of wing morph proportion and their interaction. Boxes as random effect. Box level.	Intercept	2.226	0.625	3.564	0.000365 ***
		Photoperiod 15:9	-0.0876	0.847	-0.103	0.918
		Sex ratio[a]	-0.917	1.211	-0.757	0.449
		Photoperiod 15:9 : Sex ratio[a]	-1.275	1.712	-0.745	0.456

5	Generalised linear model with random effects (GLMER). Photoperiod as predictor of wing morph proportion. Boxes as random effect. Box level.	Intercept	1.790	0.172	10.397	<2e-16 ***
		Photoperiod 15:9	-0.630	0.221	-2.856	0.00430 **
6	Generalised linear model with random effects (GLMER). Sex ratio as predictor of wing morph proportion with boxes as random effect. Box level.	Intercept	1.998	0.475	4.209	2.57e-05 ***
		Sex ratio[a]	-1.085	0.963	-1.127	0.260

* $p < 0.05$, ** $p < 0.005$, *** $p < 0.0005$.

[a] Sex ratio is defined as $M / (M + F)$, where M and F are the number of males and females in the box, respectively.

Table S5: Predicted probabilities of becoming short-winged depending on photoperiod and sex based on generalised linear model 2.

Photoperiod	Sex	Probability (%)	95% CI[a]
15:9	Female	87.3%	[0.811, 0.917]
15:9	Male	62.0%	[0.530, 0.703]
15.30:8.30	Female	93.5%	[0.884, 0.964]
15.30:8.30	Male	77.4%	[0.698, 0.835]

[a] CI = confidence interval, presented as [lower limit, upper limit].

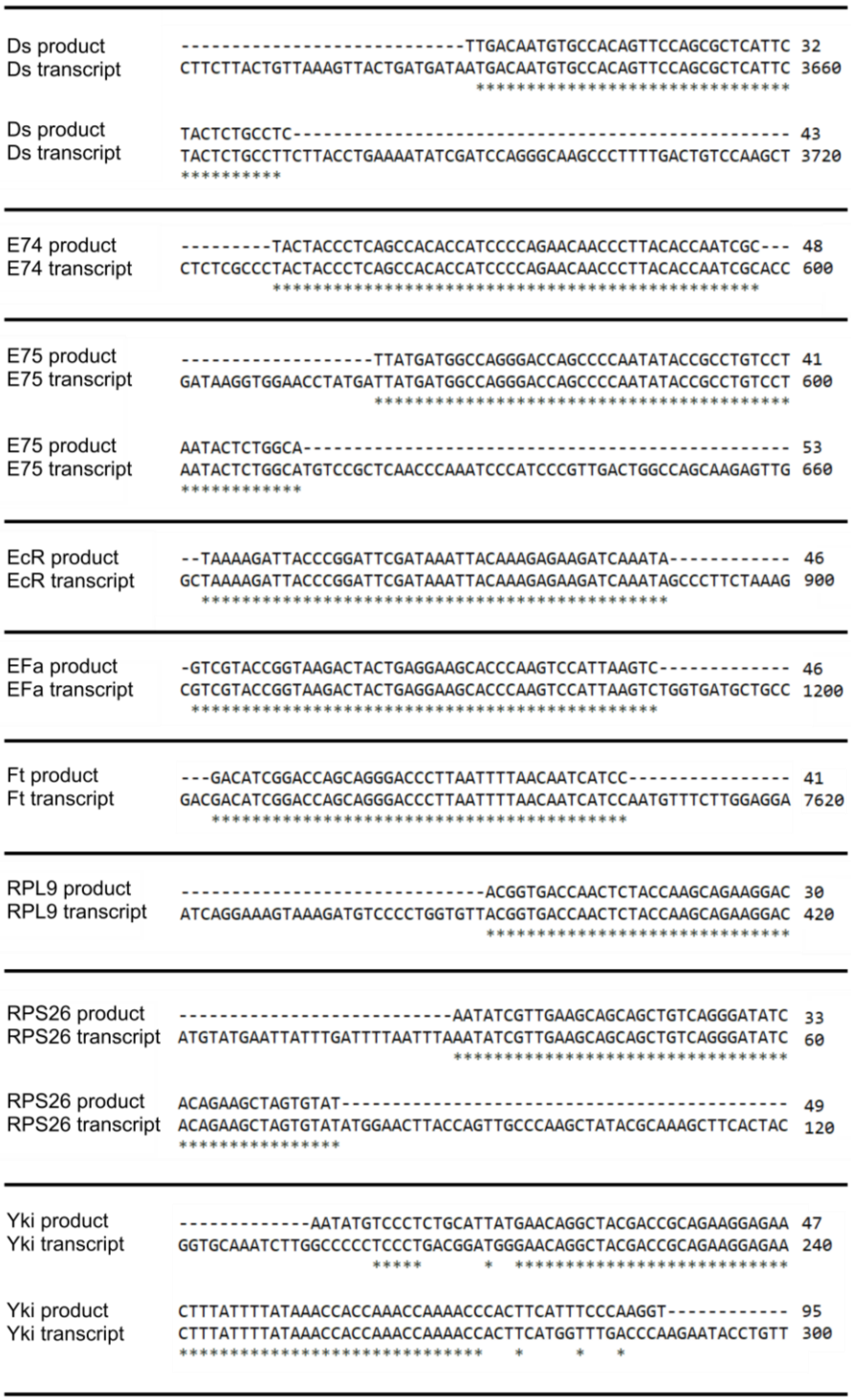

Figure S2: Alignment of Sanger sequencing products (sequence above) with target transcripts (sequence below). Alignment made using Clustal Omega (Madeira et al. 2022). Abbreviations: Ds, Dachsous; Yki, Yorkie; Ft, Fat.

Table S6: Melting temperatures of qPCR products.

Target	Melting temperature (°C)
Fat	75.50
Ds	**77.00**-77.50
EFa	78.00
Yki	**74.50**-75.00
E74	79.00
RPL9	77.00-**77.50**
RPS26	76.50
E75	**80.00**-80.50
EcR	73.00-**73.50**

Bold letters indicate the temperature that was recorded in the majority of the reactions.

Table S7: Standard curve parameters.

Target	Photoperiod	Slope	Intercept	R^2	E
Ft	12:12	-3.799	30.936	0.996	0.833
Ft	18:6	-3.772	28.873	0.970	0.841
Ds	12:12	-3.092	31.721	0.969	1.106
Ds	18:6	-3.754	30.467	0.980	0.847
EFa	12:12	-3.423	26.066	0.992	0.959
EFa	18:6	-4.012	25.064	0.992	0.775
Yki	12:12	-3.046	31.183	0.951	1.129
Yki	18:6	-3.609	30.056	0.992	0.893
E74	12:12	-3.312	32.035	0.943	1.004
E74	18:6	-4.052	30.591	0.904	0.765
RPL9	12:12	-3.632	32.532	0.895	0.885
RPL9	18:6	-4.831	32.477	0.976	0.611
RPS26	12:12	-3.846	32.190	0.956	0.820
RPS26	18:6	-3.879	31.261	0.957	0.811
E75	12:12	-3.409	29.996	0.963	0.965
E75	18:6	-3.926	28.612	0.990	0.798
EcR	12:12	-2.937	33.584	0.812	1.190
EcR	18:6	-4.425	31.803	0.933	0.683